



Thermo-mechanical analysis of functionally graded thick spheres with linearly time-dependent temperature

A. Bayat^a, H. Moosavi^a and Y. Bayat^{b,*}

a. *Department of Mechanical Engineering, Esfahan University of Technology, Esfahan, Iran.*

b. *Faculty of Engineering, Ferdowsi University of Mashhad, Mashhad, 9177948944-11, Iran.*

Received 19 November 2012; received in revised form 3 November 2014; accepted 1 December 2014

KEYWORDS

Thick-walled sphere;
 FGM;
 FEM;
 Linearly time-dependent temperature.

Abstract. An analysis of the unsteady-state thermo-mechanical problem of functionally graded thick-walled spheres is presented in this paper. The material properties, except Poisson's ratio, are assumed to be an arbitrary function of radial direction. Considering linearly increasing boundary temperature and employing Laplace transform techniques, the time-dependent temperature is obtained. In a special case, by assuming the material properties to follow a power-law function, the Navier equation is solved for an arbitrary time. This led to radial displacement, radial stress, and hoop stress as a function of radial direction. In the numerical results calculated by FEM software, ABAQUS is compared to the analytical results. The present results agree well with existing analytical results.

© 2015 Sharif University of Technology. All rights reserved.

1. Introduction

Spheres heated by their surrounding are omnipresent in most common engineering design structures. The engineering relevance of the heat source for cylinder or sphere vessels can be considered as hot fluid or hot gas flow in the vessel at the chemical operations in reactors [1]. The analytical solutions of various heat conduction problems, such as axisymmetric, non-axisymmetric, steady state and transient heat conduction for isotropic thick hollow spheres in the elastic stress state, are available in advanced textbooks and articles [2-10].

Recently, a new class of composite materials, known as Functionally Graded Materials (FGMs), are used as heat-shielding materials. The possibility of tailoring the desired thermo-mechanical properties holds enormous application potential for FGMs. In fact, these materials are made of a mixture, with arbitrary composition of two different materials; the volume

fraction of each material changing continuously and gradually. The ability to tailor a composition with low thermal conductivity, low coefficient of thermal expansion and core ductility have enabled the FGM materials to withstand higher temperature gradients for a given heat flux. Examples of structures that undergo extremely high temperature gradients are plasma facing materials, the propulsion system of planes, cutting tools, engine exhaust liners, aerospace skin structures, incinerator linings, thermal barrier coating of turbine blades, thermal resistant tiles, and directional heat flux materials [11]. Used continuously, varying the volume fraction of the mixture in the FGM can control the stress profile in these structures, such that the interface problems and mitigating thermal stress concentrations are eliminated. Thus, heat conduction analysis of FGMs is of great interest. Solution of the temperature field is essential to calculating thermal stresses within the structures. Obata and Noda [12] studied one-dimensional steady thermal stresses in a functionally graded circular hollow cylinder and a hollow sphere using the perturbation method. Nayebi and EI Abdi [13] developed a numerical program to

*. *Corresponding author. Tel.: +98 935 4724912
 E-mail address: y.bayat.mech@gmail.com (Y. Bayat)*

investigate the steady state behavior of thick walled spherical and cylindrical pressure vessels subjected to cyclic pressure and/or temperature. Actually, the steady-state heat conduction problems in thick spheres made of FGM have been investigated in several pieces of literature [14–18]. However, there are a broad range of practical applications, especially operating at large temperature drops in which, in some cases, the transient thermal stresses are large enough to cause structural failure. Therefore, analysis of transient heat conduction with various initial problem conditions for spherical vessels made of FGMs has attracted widespread attention over the past ten years. For instance, Ootao et al. [19] derived the three-dimensional transient thermal stresses of a non-homogeneous hollow sphere, with respect to a rotating heat source. Using a combined analytical and numerical method, Tsai and Hung [20] investigated the thermal wave propagation in an abi-layered composite sphere, due to a sudden temperature change on the outer surface. Non-Fourier hyperbolic heat conduction in a heterogeneous sphere made of FGMs was investigated by Babaei and Chen [21]. In this work, the problem is solved analytically in the Laplace domain, and the final results in the time domain are obtained using the numerical inverse of the Laplace transform. Ghosh and Kanoria [22] considered the analysis of thermo-elastic response in a functionally graded spherically isotropic hollow sphere based on the Green-Lindsay theory. They assumed that the inner surface was subjected to a time-dependent thermal shock, whereas the outer surface was maintained at constant temperature. Thermo-elastic analysis of a functionally graded orthotropic hollow sphere under thermal shock with a three-phase-lag effect was carried out by Kar and Kanoriab [23]. In another work, magneto-thermo-elastic transient response of a functionally graded thick hollow sphere, subjected to magnetic and thermo-elastic fields, was obtained by Ghorbanpour et al. [24]. Besides, Ootao and Ishihara [25] developed the transient thermal stress problem of a functionally graded magneto-electro-thermo-elastic hollow sphere. Furthermore, the temperature field and stress-strain state caused by time-dependent temperature boundary conditions for cylindrical vessels made of FGMs were determined by Shao and Ma [26].

The objective of the present study is to analyze the thick-walled spherical vessels made of FGMs subjected to mechanical and linear time-dependent thermal loadings. In other words, the temperature of the inner surface rises linearly from zero to the steady-state temperature, and the outer surface temperature is kept constant. The thermo-mechanical properties of Functionally Graded Material (FGM) are assumed to vary continuously in the radial direction. To derive the time-dependent temperature, the ordinary

differential equations are solved by implementing the Laplace transform technique and power series method. Expressing the temperature distribution as a power series, the Navier equation has been solved at an arbitrary time. Finally, using ABAQUS simulations, the finite element method is compared with the analytical results.

2. Thermo elastic analysis of FGM hollow spheres

Consider a radially graded FGM hollow sphere whose inner and outer radii are R_1 and R_2 , respectively. The surfaces of the body are subjected to uniform pressure, P_1 and P_2 , on the inner and outer surfaces, respectively. Besides, the inner surface is heated such that its temperature rises linearly from zero to a constant temperature, T_1 , as shown in Figure 1. The outer surface temperature is kept at a constant temperature, T_2 . Moreover, it is assumed that neither body forces nor heat generation are acting inside the medium. For the analysis, the following dimensionless quantities are introduced:

$$\begin{aligned} r &= R/R_m, \quad r_1 = R_1/R_m, \quad r_2 = R_2/R_m, \\ E^* &= E/E_0, \quad \alpha^* = \alpha/\alpha_0, \quad \lambda^* = \lambda/\lambda_0, \quad k^* = k/k_0, \\ T^* &= T/T_0, \quad \tau = k_0 t/R_m^2, \quad H_2 = R_m h_2/\lambda_0, \\ u^* &= u/\alpha_0 T_0 R_m, \quad \sigma_r^* = \sigma_R/\alpha_0 T_0 E_0, \\ \sigma_\theta^* &= \sigma_\theta/\alpha_0 T_0 E_0, \quad P_1^* = P_1/\alpha_0 E_0 T_0, \\ P_2^* &= P_2/\alpha_0 E_0 T_0, \end{aligned} \quad (1)$$

where R_m is the mean radius, which is defined as: $R_m = (R_1 + R_2)/2$, and T_0 is the reference temperature. Also, k_0, λ_0, α_0 and E_0 are reference values of thermal diffusivity, thermal conductivity, coefficient of thermal expansion, and the modulus of elasticity, respectively. Actually, the corresponding radius of k_0, λ_0, α_0 and E_0

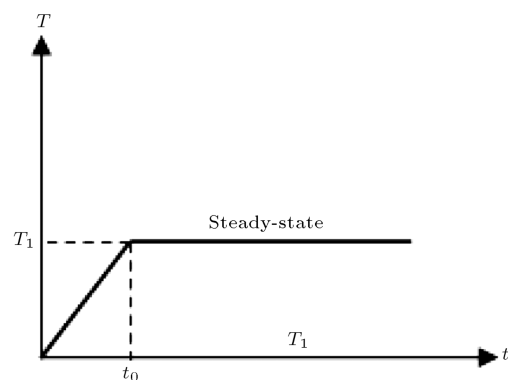


Figure 1. Linearly increasing temperature in the inner surface of hollow sphere.

are the material properties of the hollow sphere. Besides, H_2 is the dimensionless heat transfer conduction on the outer surface. It should be mentioned that $k_0 = \lambda_0/\rho_0 C_{p0}$, in which C_{p0} is the specific heat of the vessel at mean radius.

Using the dimensionless displacement, u^* , the strain-displacement relations can be written as:

$$\varepsilon_r^* = \frac{du^*}{dr}, \tag{2a}$$

$$\varepsilon_\theta^* = \frac{u^*}{r}. \tag{2b}$$

The dimensionless stress-strain relations are:

$$\sigma_r^* = \frac{E^*(r)}{(1+v)(1-2v)} [(1-v)\varepsilon_r^* + 2v\varepsilon_\theta^* - (1+v)\alpha^*(r)T^*(r, \tau)], \tag{3a}$$

$$\sigma_\theta^* = \frac{E^*(r)}{(1+v)(1-2v)} [v\varepsilon_r^* + \varepsilon_\theta^* - (1+v)\alpha^*(r)T^*(r, \tau)], \tag{3b}$$

where v is Poisson’s ratio. The equilibrium equation is:

$$\frac{d\sigma_r^*}{dr} + \frac{2}{r}(\sigma_r^* - \sigma_\theta^*) = 0. \tag{4}$$

Substitution of Eqs. (2) and (3) into Eq. (4) produces the Navier equation:

$$\begin{aligned} \frac{\partial^2 u^*(r, \tau)}{\partial r^2} + \left(\frac{2}{\rho} + \frac{(E^*(r))'}{E^*(r)} \right) \frac{\partial u^*(r, \tau)}{\partial r} \\ + 2 \left(\frac{\nu}{1-\nu} \frac{(E^*(r))'}{E^*(r)} - \frac{1}{r} \right) \\ = \frac{1+\nu}{1-\nu} \alpha^*(r) \left(\frac{(\alpha^*(r)E^*(r))'}{\alpha^*(r)E^*(r)} T^*(r, \tau) \right. \\ \left. + (T^*(r, \tau))' \right), \end{aligned} \tag{5}$$

where $()'$ denotes the derivative with respect to r .

3. Heat of transition in the FGM thick walled sphere

In the absence of heat sources, the heat conduction equation is expressed as follows:

$$\begin{aligned} \frac{\partial^2 T^*(r, \tau)}{\partial r^2} + \left(\frac{2}{r} + \frac{(\lambda^*(r))'}{\lambda^*(r)} \right) \frac{\partial T^*(r, \tau)}{\partial r} \\ = \frac{1}{k^*(r)} \frac{\partial T^*(r, \tau)}{\partial \tau}. \end{aligned} \tag{6}$$

Considering Figure 1, initial and boundary conditions

are expressed as follows:

$$T^*(r, 0) = 0, \tag{7}$$

$$r = r_1 : T^* = \begin{cases} T_1^* \frac{\tau}{\tau_0}, & 0 \leq \tau \leq \tau_0 \\ T_1^*, & \tau > \tau_0 \end{cases} \tag{8a}$$

$$r = r_2 : k^*(r) \frac{\partial T^*(r_2, \tau)}{\partial r} + H_2 T^*(r_2, \tau) = H_2 T_2^*. \tag{8b}$$

Firstly, the solution for the phase of $0 \leq \tau \leq \tau_0$ is derived. Similar to [26], performing Laplace transformation, in terms of τ , to Eq. (6) and boundary conditions in Eqs. (8), the governing equations of the problem in the Laplace domain can be obtained as:

$$\begin{aligned} \frac{\partial^2 F(r, s)}{\partial r^2} + \left(\frac{2}{r} + \frac{(\lambda^*(r))'}{\lambda^*(r)} \right) \frac{\partial F(r, s)}{\partial r} \\ = \frac{1}{k^*(r)} [sF(r, s)], \end{aligned} \tag{9}$$

$$r = r_1 : F = \frac{T_1^*}{\tau_0} \frac{1}{s^2}, \tag{10a}$$

$$r = r_2 : \frac{\partial F(r, s)}{\partial r} + H_2 F(r, s) = \frac{1}{s} H_2 T_2^*. \tag{10b}$$

Regarding the series method for solving ordinary differential equations, coefficients $2/r$, $(\lambda^*(r))'/\lambda^*(r)$ and $1/k^*(r)$, are analytical at $r = 1$. So, the Taylor series about this point can be written as:

$$\frac{2}{r} = \sum_{n=0}^{\infty} (-1)^n (r-1)^n, \tag{11a}$$

$$\frac{(\lambda^*(r))'}{\lambda^*(r)} = f_1(r) = \sum_{n=0}^{\infty} f_{1,n} (r-1)^n, \tag{11b}$$

$$\frac{1}{k^*(r)} = f_2(r) = \sum_{n=0}^{\infty} f_{2,n} (r-1)^n, \tag{11c}$$

where:

$$f_{1,n} = \frac{1}{n!} f_1^n(1), \tag{12a}$$

$$f_{2,n} = \frac{1}{n!} f_2^n(1). \tag{12b}$$

Using the series to solve Eq. (9), the solution can be expressed as follows:

$$F(r, s) = \sum_{n=0}^{\infty} A_n (r-1)^n. \tag{13}$$

Substituting Eqs. (13) and (11) into Eq. (9) and comparing the coefficients of $(r-1)^n$ gives the recurrence

relation as:

$$\begin{aligned} &(n + 2)(n + 1)A_{n+2} + 2 \sum_{i=0}^n (-1)^{n-i}(i+1)A_{i+1} \\ &+ \sum_{i=0}^n f_{1,n-i}(i + 1)A_{i+1}(r - 1)^n \\ &= s \sum_{i=0}^n f_{2,n-i}A_i(r - 1)^n. \end{aligned} \tag{14}$$

In the above equation, coefficients A_n are the linear combination of A_0 and A_1 , which can be written as follows:

$$A_n(s) = d_{1,n}(s)A_0 + d_{2,n}(s)A_1, \tag{15}$$

where the coefficients of $d_{1,n}(s)$ and $d_{2,n}(s)$ are obtained from Eq. (14). Thus, Eq. (13) can be rewritten as:

$$F(r, s) = \sum_{n=0}^{\infty} (A_0d_{1,n}(s) + A_1d_{2,n}(s))(r - 1)^n, \tag{16}$$

where A_0 and A_1 are unknown constants that can be obtained by the use of the boundary conditions. To calculate the unknown constants, Eq. (16) is substituted into the boundary conditions in Eqs. (10):

$$\begin{pmatrix} a_{11} & a_{12} \\ a_{21} & a_{22} \end{pmatrix} \begin{pmatrix} A_0 \\ A_1 \end{pmatrix} = \begin{pmatrix} \frac{T_1^*}{\tau_0} \frac{1}{s^2} \\ \frac{H_2 T_2^*}{s} \end{pmatrix}, \tag{17}$$

where:

$$a_{11} = \sum_{n=0}^{\infty} d_{1,n}(s)(r_1 - 1)^n, \tag{18a}$$

$$a_{12} = \sum_{n=0}^{\infty} d_{2,n}(s)(r_1 - 1)^n, \tag{18b}$$

$$\begin{aligned} a_{21} &= \sum_{n=0}^{\infty} (n + 1)d_{1,n+1}(s)(r_2 - 1)^n \\ &+ H_2 \sum_{n=0}^{\infty} d_{1,n}(s)(r_2 - 1)^n, \end{aligned} \tag{18c}$$

$$\begin{aligned} a_{22} &= \sum_{n=0}^{\infty} (n + 1)d_{2,n+1}(s)(r_2 - 1)^n \\ &+ H_2 \sum_{n=0}^{\infty} d_{2,n}(s)(r_2 - 1)^n. \end{aligned} \tag{18d}$$

Coefficients A_0 and A_1 can easily be extracted from

Eq. (17):

$$A_0 = \frac{1}{s^2} \frac{\det \begin{pmatrix} \frac{T_1^*}{\tau_0} & a_{12} \\ H_2 T_2^* s & a_{22} \end{pmatrix}}{\det \begin{pmatrix} a_{11} & a_{12} \\ a_{21} & a_{22} \end{pmatrix}}, \tag{19a}$$

$$A_1 = \frac{1}{s^2} \frac{\det \begin{pmatrix} a_{11} & \frac{T_1^*}{\tau_0} \\ a_{21} & H_2 T_2^* s \end{pmatrix}}{\det \begin{pmatrix} a_{11} & a_{12} \\ a_{21} & a_{22} \end{pmatrix}}. \tag{19b}$$

Substituting Eq. (19) into Eq. (16) yields:

$$F(R, s) = \sum_{n=0}^{\infty} \frac{N_n(s)}{M(s)}(r - 1)^n, \tag{20}$$

where:

$$\begin{aligned} N_n(s) &= \det \begin{pmatrix} \frac{T_1^*}{\tau_0} & a_{12} \\ H_2 T_2^* s & a_{22} \end{pmatrix} d_{1,n}(s) \\ &+ \det \begin{pmatrix} a_{11} & \frac{T_1^*}{\tau_0} \\ a_{21} & H_2 T_2^* s \end{pmatrix} d_{2,n}(s), \end{aligned} \tag{21a}$$

and

$$M(s) = s^2 \det \begin{pmatrix} a_{11} & a_{12} \\ a_{21} & a_{22} \end{pmatrix}. \tag{21b}$$

The dimensionless $T^*(r, \tau)$ can be derived by using the inverse Laplace transform for all coefficients of $(r - 1)^n$ in Eq. (20). In this way, the roots of equation $M(s) = 0$ can be simple or multiple-root. Hereby, in the case where equation $M(s) = 0$ has only simple roots, $k(k = 1, 2, \dots, n)$, the inverse transform of Eq. (20) can be written as:

$$T^*(r, \tau) = \sum_{n=0}^{\infty} \left(\sum_{j=1}^k \frac{N_n(s_j)}{\left(\frac{dM(s)}{ds} \right)_{s=s_j}} e^{s_j \tau} \right) (r - 1)^n, \tag{22}$$

while in the case where equation $M(s) = 0$ has multiple-roots with j orders, and $s_{j+1}, s_{j+2}, s_{j+3} \dots$ are single roots of function $M(s)$, the solution can be obtained as:

$$\begin{aligned} T^*(r, \tau) &= \sum_{n=0}^{\infty} \left(\frac{1}{(j - 1)!} \lim_{s \rightarrow s_1} \frac{d^{j-1}}{ds^{j-1}} \right. \\ &\left. \left((s - s_1)^j \frac{N_n(s)}{M(s)} e^{s\tau} \right) \right. \\ &\left. + \sum_{p=j+1}^k \frac{N_n(s_k)}{\left(\frac{dM(s)}{ds} \right)_{s=s_p}} e^{s_p \tau} \right) (r - 1)^n. \end{aligned} \tag{23}$$

For phase $\tau_0 < \tau$, the temperature is obtained by

following the work of [4], as:

$$T^* = T^*(r, \tau) - T^*(r, \tau - \tau_0), \tag{24}$$

where $T^*(r, \tau - \tau_0)$ is a function similar to $T^*(r, \tau)$ in which τ takes the place of $\tau - \tau_0$.

4. Solution of the Navier equation with the heat of transition

By substituting the temperature distribution obtained in Eqs. (22) or (23) into the Navier equation, and solving this equation, displacements and stress distribution can be derived. For this purpose, considering Eqs. (22) and (23), the temperature distribution can also be expressed at an arbitrary time as follows:

$$T^*(r) = a_0 + a_1 r + a_2 r^2 + a_3 r^3 + \dots + a_i r^i = \sum_{i=0}^{\infty} a_i r^i. \tag{25}$$

Using a comparison of extended Eqs. (22) or (23) with Eq. (25), coefficients a_0, a_1, \dots, a_i can be obtained. Substituting equation (25) into the Navier equation (5) gives:

$$\begin{aligned} \frac{\partial^2 u^*(r)}{\partial r^2} + \left(\frac{2}{\rho} + \frac{(E^*(r))'}{E^*(r)} \right) \frac{\partial u^*(r)}{\partial r} \\ + 2 \left(\frac{\nu}{1-\nu} \frac{(E^*(r))'}{E^*(r)} - \frac{1}{r} \right) \\ = \frac{1+\nu}{1-\nu} \alpha^*(r) \left(\frac{(\alpha^*(r)E^*(r))'}{\alpha^*(r)E^*(r)} \sum_{i=0}^{\infty} a_i r^i \right. \\ \left. + \sum_{i=1}^{\infty} i a_i r^{i-1} \right). \end{aligned} \tag{26}$$

In a special case, the sphere's material is assumed to be graded through the thickness, where the material properties are approximated with the power-law functions as:

$$E(r) = E_0 r^{\beta_1}, \tag{27a}$$

$$\alpha(r) = \alpha_0 r^{\beta_2}, \tag{27b}$$

$$\lambda(r) = \lambda_0 r^{\beta_3}, \tag{27c}$$

$$k(r) = k_0 r^{\beta_4}. \tag{27d}$$

Substituting Eq. (27) into Eq. (26), the Navier equation can be rewritten:

$$\begin{aligned} r^2 (u^*(r))'' + Ar (u^*(r))' + Bu(r) = Cr^{\beta_2+1} \\ \sum_{i=0}^{\infty} a_i r^i + Dr^{\beta_2+2} \sum_{i=0}^{\infty} (i+1) a_{i+1} r^i, \end{aligned} \tag{28}$$

where:

$$\begin{aligned} A = 2 + \beta_1, \quad B = \frac{2[\nu(\beta_1 + 1) - 1]}{1 - \nu}, \\ C = \frac{1 + \nu}{1 - \nu}(\beta_1 + \beta_2), \quad D = \frac{1 + \nu}{1 - \nu}. \end{aligned} \tag{29}$$

Eq. (28) is a non-homogeneous Euler differential equation with general and particular solutions whose complete solution, $u^*(r)$, is:

$$\begin{aligned} u^*(r) = c_1 r^{m_1} + c_2 r^{m_2} + c_3 r^{\beta_2+1} \sum_{i=0}^{\infty} a_i r^i \\ + c_4 r^{\beta_2+1} \sum_{i=1}^{\infty} i a_i r^i, \end{aligned} \tag{30}$$

where $m_{1,2}$ are given by a homogeneous solution as follows:

$$m_{1,2} = \frac{1 - A \pm \sqrt{\Delta}}{2}, \tag{31a}$$

$$\Delta = (A - 1)^2 - 4B. \tag{31b}$$

Substituting particular solutions into Eq. (28) yields:

$$\begin{aligned} c_3 \sum_{i=2}^{\infty} (i + \beta_2)(i + \beta_2 + 1) a_i r^i + c_4 \sum_{i=3}^{\infty} i(i + \beta_2) \\ (i + \beta_2 + 1) a_i r^i + A \left(c_3 \sum_{i=1}^{\infty} (i + \beta_2 + 1) a_i r^i \right. \\ \left. + c_4 \sum_{i=1}^{\infty} i(i + \beta_2 + 1) a_i r^i \right) + B \left(c_3 \sum_{i=0}^{\infty} a_i r^i \right. \\ \left. + c_4 \sum_{i=1}^{\infty} i a_i r^i \right) = C \sum_{i=0}^{\infty} a_i r^i + D \sum_{i=1}^{\infty} i a_i r^i. \end{aligned} \tag{32}$$

Using Eq. (32), coefficients c_3 and c_4 can be calculated.

By substituting Eqs. (30) and (25) into Eqs. (2) and (3), the resulting stress expressions are:

$$\begin{aligned} \sigma_r^*(r) = \frac{r^{\beta_1}}{(1 + \nu)(1 - 2\nu)} \left[r^{m_1-1} c_1 (2\nu + (1 - \nu)m_1) \right. \\ \left. + r^{m_2-1} c_2 (2\nu + (1 - \nu)m_2) + r^{\beta_2} c_3 \right. \\ \left. \left(2\nu \sum_{i=0}^{\infty} a_i r^i + (1 - \nu) \sum_{i=1}^{\infty} (i + \beta_2 + 1) a_i r^i \right) \right. \\ \left. + r^{\beta_2} c_4 \left(2\nu \sum_{i=1}^{\infty} i a_i r^i + (1 - \nu) \sum_{i=2}^{\infty} i(i + \beta_2) a_i r^i \right) \right. \\ \left. - r^{\beta_2} (1 + \nu) \sum_{i=0}^{\infty} a_i r^i \right], \end{aligned} \tag{33a}$$

$$\begin{aligned} \sigma_{\theta}^*(r) = & \frac{r^{\beta_1}}{(1+\nu)(1-2\nu)} \left[r^{m_1-1} c_1 (1+\nu m_1) \right. \\ & + r^{m_2-1} c_2 (1+\nu m_2) + r^{\beta_2} c_3 \left(\sum_{i=0}^{\infty} a_i r^i \right. \\ & \left. + \nu \sum_{i=1}^{\infty} (i+\beta_2+1) a_i r^i \right) \\ & + r^{\beta_2} c_4 \left(\sum_{i=1}^{\infty} i a_i r^i + \nu \sum_{i=2}^{\infty} i(i+\beta_2) a_i r^i \right) \\ & \left. - r^{\beta_2} (1+\nu) \sum_{i=0}^{\infty} a_i r^i \right]. \end{aligned} \quad (33b)$$

In Eq. (33), c_1 and c_2 are unknown constants that can be obtained by applying the following boundary conditions:

$$\begin{aligned} \sigma_r^*(r)|_{r=r_1} &= -P_1^*, \\ \sigma_r^*(r)|_{r=r_2} &= -P_2^*, \end{aligned} \quad (34)$$

in which, P_1^* and P_2^* are normalized pressures on the inner and outer surfaces, respectively.

5. Finite element solution

A geometry specimen is modeled using a commercial FE code, ABAQUS, for a comparative study. In the FE model, due to symmetry, only a quarter of the sphere specimen geometry is considered. An 8-node axisymmetric thermally coupled quadrilateral element is used to represent the FGM specimen. In this model, similar to [17], the variation in material properties is implemented by having 20 layers, with each layer having a constant value of material properties. The final FEM model consists of 2780 elements in total. Figure 2 illustrates the meshing region.

Boundary conditions are depicted in Figure 2. According to this figure, U_1 , U_2 and U_3 represent the displacement components in X , Y and Z directions, respectively. Actually, the nodal points along the horizontal edge passing through the center are free to move in an X direction, but are constrained from moving in the Y direction to reflect the symmetry of the sphere specimen geometry. Moreover, the inner thermal boundary conditions are applied based on the profile described in Figure 1. To do this, the amplitude tools in ABAQUS software are used to define the time-dependent temperature profile of the inner surface. Considering the linear variation of the temperature profile for $t \leq t_0$, as depicted in Figure 1, only two points are desired to define the time-dependent temperature of the inner surface in the FE model.

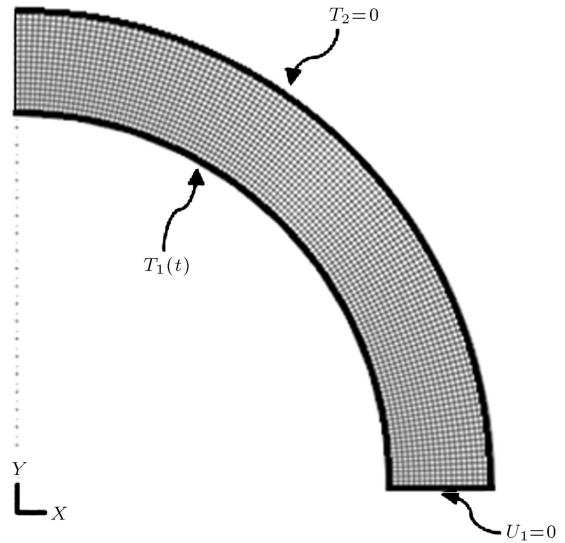


Figure 2. Finite element mesh region.

Hereby, the first and second points are assigned as $(0,0)$ and (t_0, T_1) . It should be noted that based on Figure 1, T_1 is the steady state temperature of inner radius and t_0 is the corresponding time, which can be calculated using the non-dimensional parameter, $\tau_0 = k_0 t_0 / R_m^2$. Furthermore, the temperature of the outer surface is kept constant, as shown in Figure 2.

The increment number required for the resolution is determined automatically by the software. For example, if $\beta_i (i = 1 \dots 4) = -2$, for $\tau_0 = 0.1$ and $\tau = 0.1$, the increment number will be 1066.

6. Results and discussion

The analytical and finite element analysis obtained in previous sections can be checked for a number of examples. In the following section, a case study is presented to investigate the stress and displacement responses for a thick-walled sphere under time-dependent thermal loading. Besides, in this section, FEM validation is performed by providing the numerical data.

6.1. Case study

For instance, consider a thick hollow sphere of inner radii $R_1 = 0.09$ (m) and $R_2 = 0.11$ (m), respectively. A special case is considered in which there is no heat transfer taking place between the outer surfaces and the surrounding medium ($h_2 \rightarrow \infty$). The temperature reference has been taken as $T_0 = 30^\circ\text{C}$. Moreover, it is assumed that the steady-state temperature of the inner surface, T_1 , is equal to T_0 and, correspondingly, the non-dimensional parameter, τ_0 , is 0.1. Besides, T_2 is kept constant as $T_2 = 0^\circ\text{C}$. Also, the inner and outer surfaces are assumed to be traction free, such that $P_1^* = P_2^* = 0$. The other material properties chosen for the numerical calculation in both the FE

model and analytical results are:

$$E_0 = 200(\text{GPa}), \quad \nu = 0.3, \quad \rho = 7833(\text{m}^3/\text{kg}),$$

$$\alpha_0 = 1.2 \times 10^{-6}(1/^\circ\text{C}), \quad Cp_0 = 465(\text{J}/\text{kg}\cdot^\circ\text{C}),$$

$$\lambda_0 = 54(\text{w}/\text{m}\cdot^\circ\text{C}).$$

Hence, thermal diffusivity can be calculated as $k_0 = 1.4826 \times 10^{-5} \text{ m}^2/\text{s}$. Hereby, using the non-dimensional parameter, $\tau_0 = k_0 t_0 / R_m^2$, introduced in Eq. (2), the corresponding time of the steady state temperature of the inner surface can be calculated as $t_0 = 67.4508 \text{ s}$. As discussed in Section 6, in order to model the linear variation of the time-dependent temperature of the inner surface, the first and second points are assigned as $(0,0)$ and (t_0, T_1) into the boundary condition section of the FE model. Consider a typical $\tau = 0.02$, such that $\tau < \tau_0$ and $\beta = 1$. The hoop and radial counters of the FE results are depicted in Figures 3 and 4, respectively. In these figures, s_{11} represents the radial stress, and hoop stress is demonstrated by S_{22} . It should be mentioned that the time period analysis of the FE model for this case can be calculated by $\tau = k_0 t / R_m^2$.

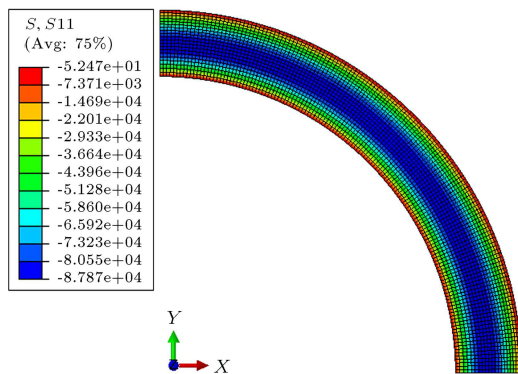


Figure 3. Contours of radial stress for $\tau = 0.02$ ($\tau < \tau_0$) and $\beta = 1$ obtained by FE model.

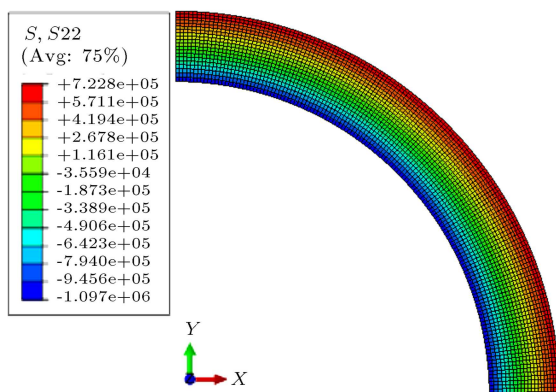


Figure 4. Contours of hoop stress for $\tau = 0.02$ ($\tau < \tau_0$) and $\beta = 1$ obtained by FE model.

Furthermore, considering the analytical non-dimensional parameters, the non-dimensional temperatures of the internal and external surrounding medium are $T_1^* = 1$ and $T_2^* = 0$, respectively. The coefficients of $d_{1,n}(s)$ and $d_{2,n}(s)$ are obtained from substituting Eq. (14) in Eq. (15). For instance, considering $n = 3$ gives:

$$\begin{aligned} d_{1,0} &= 1, & d_{1,1} &= 0, \\ d_{1,2} &= \frac{s}{2k^*(r)}, & d_{1,3} &= -\frac{s}{3k^*(r)}, \\ d_{1,4} &= \frac{s^2 + 8sk^*(r)}{24(k^*(r))^2}, & d_{1,5} &= \frac{4s^2 + 40sk^*(r)}{120(k^*(r))^2}, \\ d_{2,0} &= 0, & d_{2,1} &= 1, \\ d_{2,2} &= -1, & d_{2,3} &= \frac{6k^*(r) + s}{6k^*(r)}, \\ d_{2,4} &= -\frac{4sk^*(r) + 24(k^*(r))^2}{24(k^*(r))^2}, \\ d_{2,5} &= \frac{120(k^*(r))^2 + s^2 + 20sk^*(r)}{120(k^*(r))^2}. \end{aligned} \quad (35)$$

Substituting the coefficients obtained from Eq. (35) into Eqs. (19), the coefficients of A_0 and A_1 can easily be found. By calculating the coefficients of A_0 and A_1 , the temperature profile can be extracted. The numerical results converge rapidly by increasing with the series items. However, there are no substantial differences between the results for the series items of more than five terms. Therefore, $n = 5$ can be considered as the necessary number of terms of the series.

In the following figures, firstly, by increasing τ , the patterns of temperature, stress and displacement distribution during the inner surface heating are plotted. In these figures, the power-law index is assumed to be $\beta = 1$. In the second part, the inhomogeneity effects upon the temperature, stress and displacement distributions are investigated for the transient case ($\tau < \tau_0$) and the steady-state case ($\tau > \tau_0$).

Figure 5 includes the plot of the dimensionless transient temperature along the radial direction for the assumed initial conditions. It is observed that the temperature distributions follow the given initial conditions at the inside and outside surfaces. Figures 6 and 7 are the dimensionless temperature distribution along the radius for different power-law indices in $\tau = 0.02$ and $\tau_0 < \tau$, respectively. According to these figures, as the power-law index is increased, the temperature profile is decreased. From Figure 7, it can be seen that the patterns of steady-state temperatures

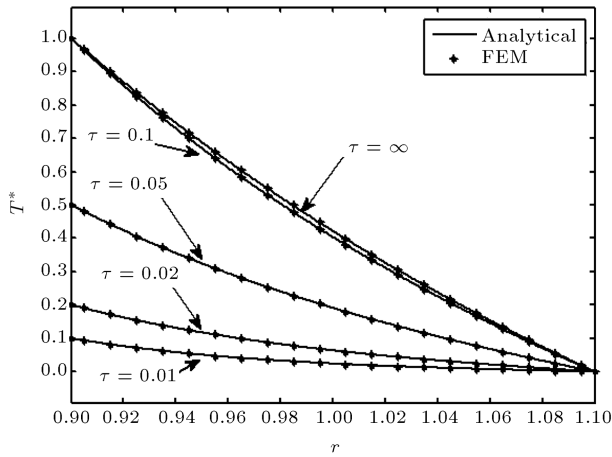


Figure 5. Distribution of dimensionless time-dependent temperature for $\beta = 1$.

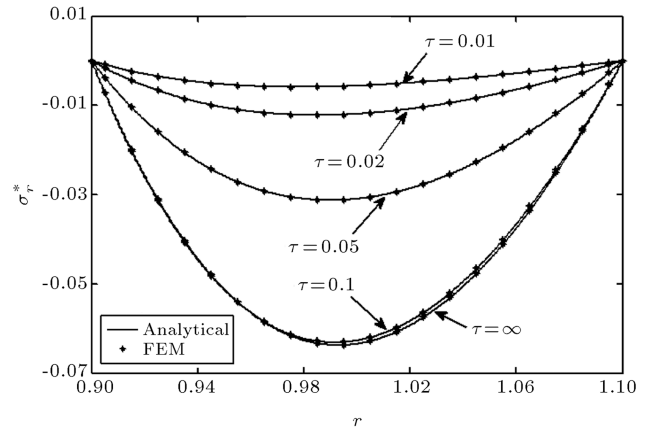


Figure 8. Distribution of dimensionless transient radial stress for $\beta = 1$.

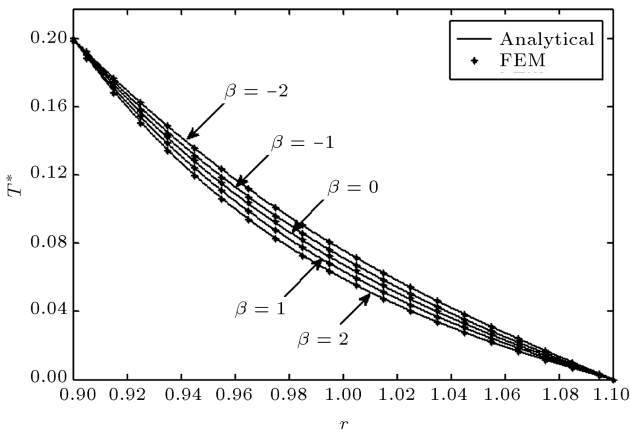


Figure 6. Distribution of dimensionless time-dependent temperature for $\tau = 0.02$.

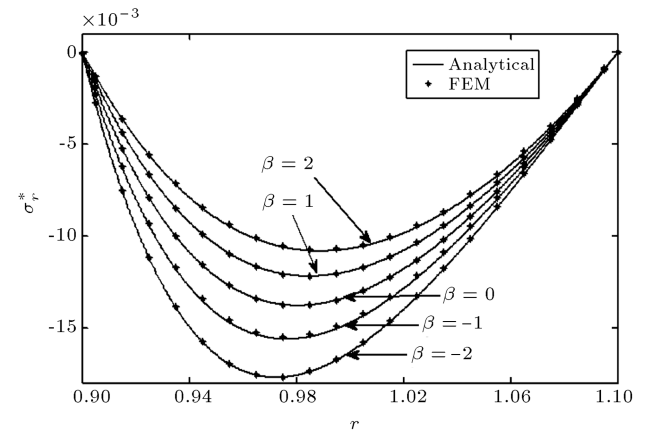


Figure 9. Distribution of dimensionless transient radial stress for $\tau = 0.02$.

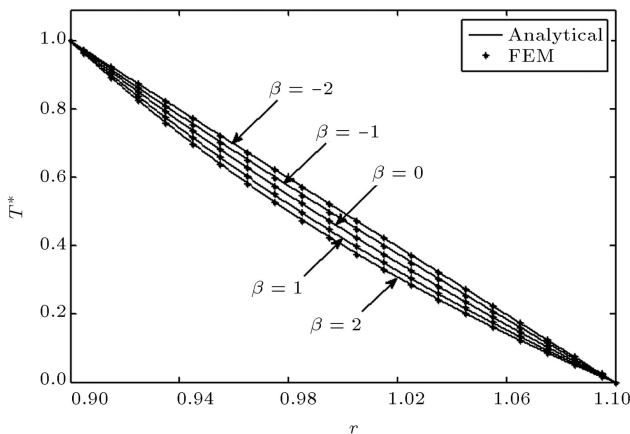


Figure 7. Distribution of dimensionless time-dependent temperature for $\tau > \tau_0$.

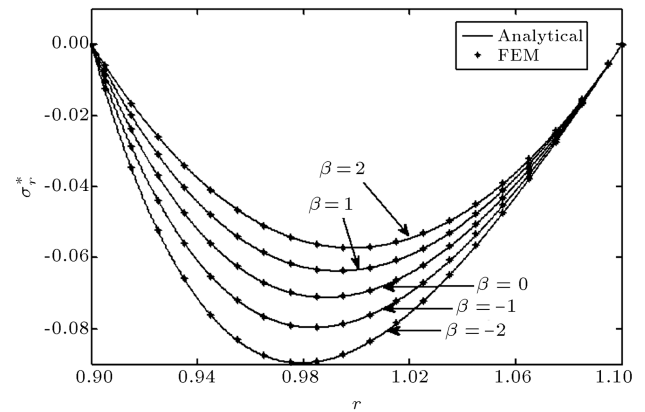


Figure 10. Distribution of dimensionless transient radial stress for $\tau > \tau_0$.

through the thickness for the steady-state case are similar to those reported in [17]. Figure 8 illustrates the dimensionless radial stress along the radial direction for $\beta = 1$ satisfying the initial thermal and the traction free mechanical boundary conditions. Figures 9 and 10

demonstrate the dimensionless radial stress for different β in $\tau = 0.02$ and $\tau_0 < \tau$, respectively. With regard to the figures, it can be stated that for higher β values, the compressive radial stresses in middle layers of the sphere increased. The steady state patterns of radial stress depicted in Figure 10 are in agreement with those reported in [17].

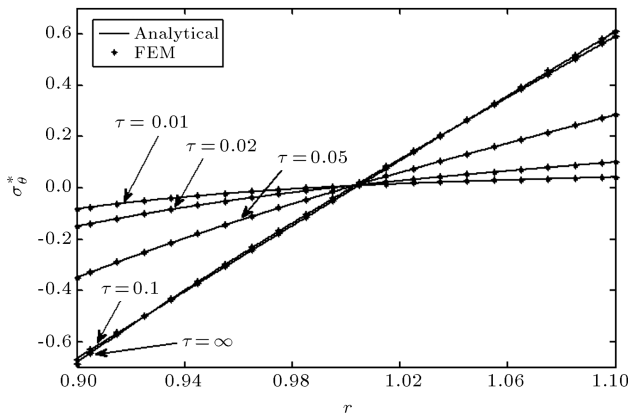


Figure 11. Distribution of dimensionless transient hoop stress for $\beta = 1$.

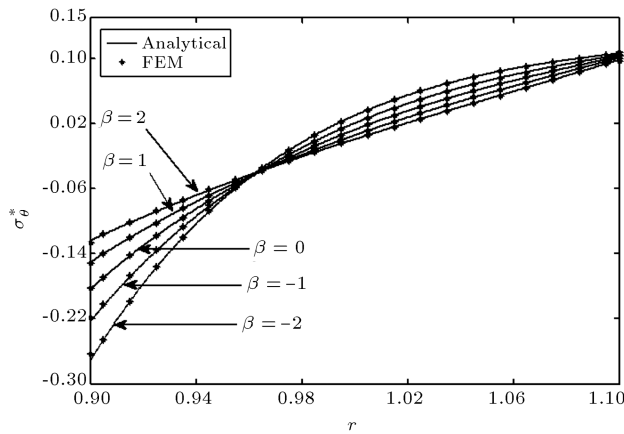


Figure 12. Distribution of dimensionless transient hoop stress for $\tau = 0.02$.

The distribution of dimensionless hoop stress for $\beta = 1$ is manifested in Figure 11. Based on this figure, the absolute values of hoop stresses increased by passing the time in the phase of $0 \leq \tau \leq \tau_0$, and rapidly approaches maximum values at the steady state in the following phase of $\tau_0 \leq \tau$. Also, distribution of dimensionless hoop stress across the radius in $\tau = 0.02$ and $\tau_0 < \tau$ for different power-law indices is represented in Figures 12 and 13, respectively. According to these figures, the hoop stress distributions are compressive at the inside surface and tensile at the outside surface. It is also observed from Figure 13 that at approximate radial distances of $r = 97$ mm and the outer surface, the stress values for all values of β converge toward the stress values in the homogenous material ($\beta = 0$). Figure 14 demonstrates the dimensionless radial displacement versus the radial direction for $\beta = 1$. Considering Figures 5, 8 and 11, similar patterns are observed for these figures too. Figures 15 and 16 are dimensionless displacement distribution along the radius for different power-law indices in $\tau = 0.02$ and $\tau_0 < \tau$, respectively. Given the information, as the power-

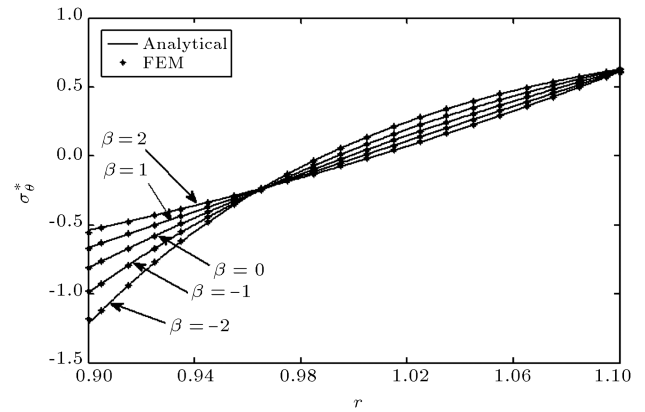


Figure 13. Distribution of dimensionless transient hoop stress for $\tau > \tau_0$.

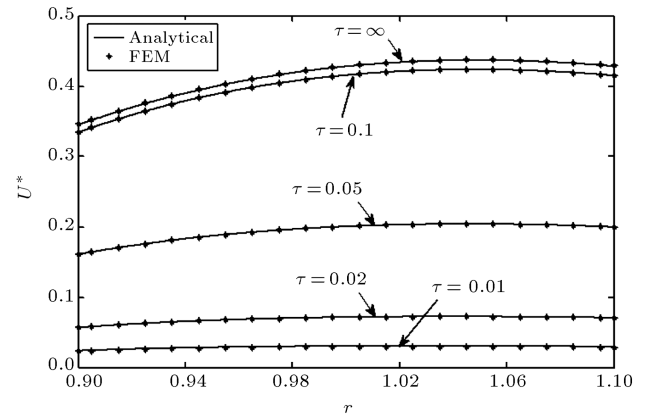


Figure 14. Distribution of dimensionless transient radial displacement for $\beta = 1$.

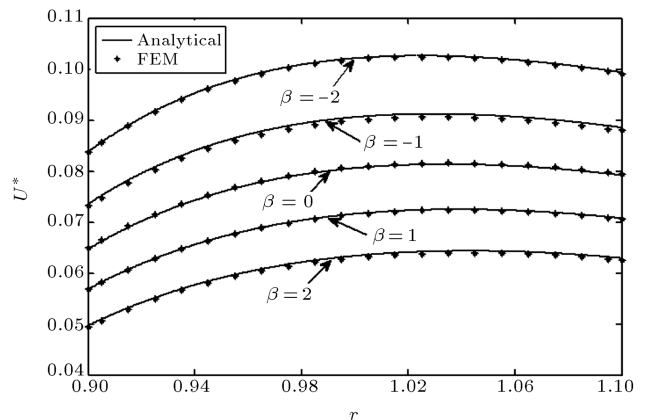


Figure 15. Distribution of dimensionless transient radial displacement for $\tau = 0.02$.

law index is increased, the displacement profile is decreased.

6.2. FEM validation

As seen in the above figures, the values of results computed by the present formulation are near to the solutions of FEM. Tables 1 and 2 compare the analytical and FEM values determined for the different

Table 1. Comparison of FE calculations with numerical data from analytical method for $\tau_0 = 0.02$ for typical $\beta = 1$.

R (mm)	Type	$T^*(r) \times 1000$		$\sigma_r^* \times 1000$		$\sigma_\theta^* \times 1000$	
		Value	%Diff	Value	%Diff	Value	%Diff
0.9	Anal.	199.768	0.1163	0	—	-149.900	1.6696
	FEM	200.001		-0.005		-152.000	
0.945	Anal.	124.152	0.0829	-9.900	0.2599	-67.800	0.1972
	FEM	124.255		-9.926		-67.900	
0.995	Anal.	68.176	0.0440	-12.100	0.3048	0.450	0.7484
	FEM	68.146		-12.063		0.453	
1.045	Anal.	30.421	0.1841	-8.400	0.6462	52.500	0.1600
	FEM	30.365		-8.346		52.600	
1.1	Anal.	0	—	0	—	100.000	0.6090
	FEM	0		-0.009		101.000	

Table 2. Comparison of FE calculations with numerical data from analytical method for steady-state ($\tau > \tau_0$) for typical $\beta = 1$.

R (mm)	Type	$T^*(r) \times 1000$		$\sigma_r^* \times 1000$		$\sigma_\theta^* \times 1000$	
		Value	%Diff	Value	%Diff	Value	%Diff
0.9	Anal.	100.000	0.0100	0	—	-663.800	1.3809
	FEM	999.900		-0.18		-672.970	
0.945	Anal.	716.500	0.1349	-48.000	0.2448	-371.000	0.0045
	FEM	717.467		-47.880		-371.020	
0.995	Anal.	446.600	0.3112	-63.700	0.0135	-50.400	0.9978
	FEM	447.990		-63.690		-50.900	
1.045	Anal.	216.400	0.4772	-47.600	0.0636	266.000	0.0924
	FEM	217.433		-47.570		265.754	
1.1	Anal.	0	—	0	—	611.700	0.2627
	FEM	0.1852		0		610.093	

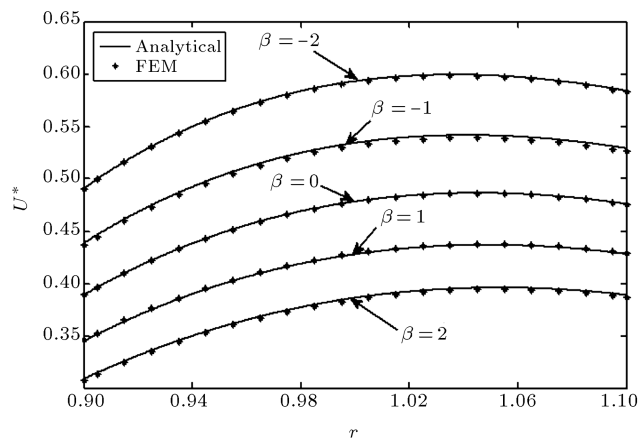


Figure 16. Distribution of dimensionless Transient radial displacement for $\tau > \tau_0$.

values of R for typical $\beta = 1$. The percentage of difference is defined as $\text{Diff}(\%) = \left| \frac{\text{Anal}-\text{FEM}}{\text{Anal}} \right| \times 100$. It is clear from the given data in Tables 1 and 2 that the $\text{Diff}(\%)$ is less than 1.7%. Actually, one can expect that for smaller divisions (more than ten layers), this difference becomes smaller.

7. Conclusions

A solution of a thick sphere made of FGMs subjected to mechanical loads and linearly increasing boundary temperature has been presented in this paper. Considering arbitrarily varying material properties in the radial direction, and employing Laplace transform techniques, the time-dependent temperature has been obtained. In a special case, assuming the material properties to follow power-law functions, the Navier equation has been solved for arbitrary time. In the numerical study, the influence of material non-homogeneity for different τ on the distribution of temperature, stress and displacement has been investigated. The results indicate that absolute values of the radial and hoop stresses increase by raising the temperature of the inner surface in the phase of $0 \leq \tau \leq \tau_0$ a, and rapidly approaches maximum values at steady state in the following phase of $\tau_0 \leq \tau$. Moreover, our results revealed that the inhomogeneity index, β , can strongly affect stress component profiles, especially hoop stress distributions. Using FEM simulations, the numerical results have been compared with analytical findings.

It is observed that the two methods results are in good agreement.

References

- Mohazzab, A.H. and Jabbari, M. "Two-dimensional stresses in a hollow FG spheres with heat source", *Advanced Materials Research*, **264-265**, pp. 700-705 (2011).
- Azadi, M. and Azadi, M. "Heat transfer-mathematical modeling, numerical methods and information technology", *In Tech*, Belmiloudi, A. pp. 253-270 (2011).
- Carslaw, H.S. and Jaeger, J.C., *Conduction of Heat in Solids*, Oxford Clarendon (1986).
- Sternberg, E. and Chakravorty, J.G. "On inertia effects in a transient thermoelastic problem", *Journal of Applied Mechanics*, **26**, pp. 503-509 (1959).
- Hopkinson, J. "Thermal stresses in a sphere, whose temperature is a function of r only", *Mess. Math*, **8**, p. 168 (1879).
- Cheung, J.B., Chen, T.S. and Thirumalai, K. "Transient thermal stresses in a sphere by local heating", *Journal of Applied Mechanics*, **41**, pp. 930-34 (1974).
- Raju, P.P. "On shallow shells of transversely isotropic materials", *Trans. ASME, Journal of Pressure Vessel Technology*, **97**, pp. 185-91 (1975).
- Timoshenko, S.P., *Strength of Materials. Part II: Advanced Theory and Problems*, D. Van Nostrand Company Inc, New York (1976).
- Takeuti, Y. and Tanigawa, Y. "Transient thermal stresses of a hollow sphere due to rotating heat source", *Journal of Thermal Stresses*, **5**, pp. 283-9 (1982).
- Wang, H.M., Ding, H.J. and Chen, W.Q. "Theoretically solution of a spherically isotropic hollow sphere for dynamic thermo-elastic problems", *Journal of Zhejiang University Science*, **4**, pp. 8-12 (2003).
- Cheung, J.B., Chen, T.S. and Thirumalai, K. "Transient thermal stresses in a sphere by local heating", *Trans. ASME, Journal of Applied Mechanics*, **41**, pp. 930-934 (1974).
- Obata, Y. and Noda, N. "Steady thermal stresses in a hollow circular cylinder and a hollow sphere of a functionally gradient material", *Journal of Thermal Stress*, **17**, pp. 471-87 (1994).
- Nayebi, A. and El Abdi, R. "Cyclic plastic and creep behavior of pressure vessels under thermo-mechanical loading", *Computational Materials Science*, **25**, pp. 285-96 (2002).
- Eslami, M.R., Babaei, M.H. and Poultangari, R. "Thermal and mechanical stresses in functionally graded thick sphere", *International Journal of Pressure Vessels and Piping*, **82**, pp. 522-527 (2005).
- Poultangari, R., Jabbari, M. and Eslami, M.R. "Functionally graded hollow spheres under non-axisymmetric thermo-mechanical loads", *International Journal of Pressure Vessels and Piping*, **85**, pp. 295-305 (2008).
- Bahtui, A., Poultangari, R. and Eslami, M.R. "Thermal and mechanical stresses in thick spheres with an extended FGM model", Brunel University Research Archive, School of Engineering and Design Research Papers (2008).
- Bayat, Y., Ghannad, M. and Torabi, H. "Analytical and numerical analysis for the FGM thick sphere under combined pressure and temperature loading", *Archive of Applied Mechanics*, **82**, pp. 229-242 (2012).
- Jabbari, M., Karampour, S. and Eslami, M.R. "Radially symmetric steady state thermal and mechanical stresses of a poro-FGM hollow sphere", *International Scholarly Research Notices*, **2011** (2011).
- Ootao, Y. and Tanigawa, Y. "Three-dimensional transient thermal stress analysis of a nonhomogeneous hollow sphere with respect to a rotating heat source", *Transactions of the Japan Society of Mechanical Engineers Series A*, **60**, pp. 2273- 2279 (1994).
- Tsai, C.S. and Hung, C. "Heat mass transfer", *International journal of heat transfer*, **46**, pp. 5137-5144 (2003).
- Babaei, M.H. and Chen, Z.T. "Hyperbolic heat conduction in a functionally graded hollow sphere", *International Journal of Thermophysics*, **29**, pp. 1457-1469 (2008).
- Ghosh, M.K. and Kanoria, M. "Analysis of thermoelastic response in a functionally graded spherically isotropic hollow sphere based on Green-Lindsay theory", *Actamechanica*, **207**, pp. 51-67 (2009).
- Kar, A. and Kanoriab, M. "Generalized thermoelastic functionally graded orthotropic hollow sphere under thermal shock with three-phase-lag effect", *European Journal of Mechanics A/Solids*, **28**, pp. 757-67 (2009).
- Ghorbanpour, A., Salari, M., Khademizadeh, H. and Arefmanesh, A. "Magnetothermoelastic transient response of a functionally graded thick hollow sphere subjected to magnetic and thermoelastic fields", *Archive of Applied Mechanics*, **79**, pp. 481-497 (2009).
- Ootao, Y. and Ishihara, M. "Transient thermal stress problem of a functionally graded magneto-electrothermoelastic hollow sphere", *Materials*, **4**, pp. 2136-2150 (2011).
- Shao, Z.S. and Ma, G.W. "Thermo-mechanical stresses in functionally graded circular hollow cylinder with linearly increasing boundary temperature", *Composite Structures*, **83**, pp. 259-265 (2008).

Biographies

Ammar Bayat obtained a BS degree in Mechanical Engineering from the University of Sistan and Baluchestan, Iran, in 2009, and an MS degree from Esfahan University of Technology, Iran, in 2011, also in Mechanical Engineering. He is currently a PhD degree candidate at Tarbiat Modares University, Tehran, Iran, undertaking impact analysis of concrete polymer as

his main study area. His research interests include stress analysis of concrete polymer and sandwich panels.

Hasan Moosavi obtained BS and MS degrees in Mechanical Engineering from the University of New Hampshire, USA, in 1983 and 1985, respectively, and a PhD degree in Mechanical Engineering from Wichita State University, USA, in 1990. He is currently faculty member of the Mechanical Engineering Department at Isfahan University of Technology, Iran. His research interests include dynamics, robotics and optimization.

He has published several ISI papers in areas such as thermal science and solid mechanics.

Yahya Bayat obtained his BS degree from the University of Sistan and Baluchestan, Iran, in 2008, and his MS degree from Shahrood University of Technology, Iran, in 2011, both in Mechanical Engineering. He is currently a PhD degree student in Solid Mechanical Engineering at Ferdowsi University, Mashhad, Iran. His research interests are in the area of stress analysis of pressure vessels, plates and shells made of high-tech materials.